TRANSPORT PROPERTIES OF ALKALI-FULLERIDES

A. ZETTL
Department of Physics, University of California at Berkeley,
and Materials Sciences Division, Lawrence Berkeley National Laboratory,
Berkeley, California 94720 U.S.A.

The normal state transport properties of the alkali-metal-doped fullerides are reviewed. Dc resistivity, Hall effect, and thermoelectric power measurements performed on single crystal specimens of A_3C_{60} are examined within different conduction models and characteristic electronic parameters are extracted. These parameters place constraints on the superconductivity mechanism. In polymerized A_1C_{60}, dc resistivity measurements suggest a rich phase diagram with possible low temperature density wave ground states.

1 Introduction

The C_{60} molecule is the basis for a host of interesting electronic materials. Alkali-intercalated C_{60} compounds of the form A_3C_{60} display superconductivity with transition temperatures T_c exceeding 30K. The suprisingly high T_c suggests either a fortunate combination of modest density of states, high-frequency phonons, and good electron coupling, or a novel superconductivity mechanism. Normal state transport measurements are a reliable method for determining relevant model parameters. Polymerized A_1C_{60} materials have a linear-chain-like structure suggestive of anisotropic conduction. Because of the lower dimensionality, these materials may also be susceptible to density wave or other instabilities at lower temperature. Transport measurements, in conjunction with other measurements such as structural, magnetic, photoemission, and spin resonance, are again essential tools in characterizing the electronic states of these unusual polymers.

Although a wide variety of alkali-fullerenes has been synthesized, few materials have been extensively characterized by transport measurements. In the case of three-dimensional alkali-fullerides, K_3C_{60} and Rb_3C_{60} have been the most carefully studied. In this report we shall focus on dc transport measurements on single crystal K_3C_{60} and Rb_3C_{60}. For the polymerized materials, we review dc transport in K_1C_{60}, Rb_1C_{60}, and Cs_1C_{60}.

2 Transport in K_3C_{60} and Rb_3C_{60} Crystals

2.1 Dc Resistivity

Fig. 1 shows the normalized dc electrical resistivity[1,2] of single crystal specimens of K_3C_{60} and Rb_3C_{60} below 250K. Although the functional

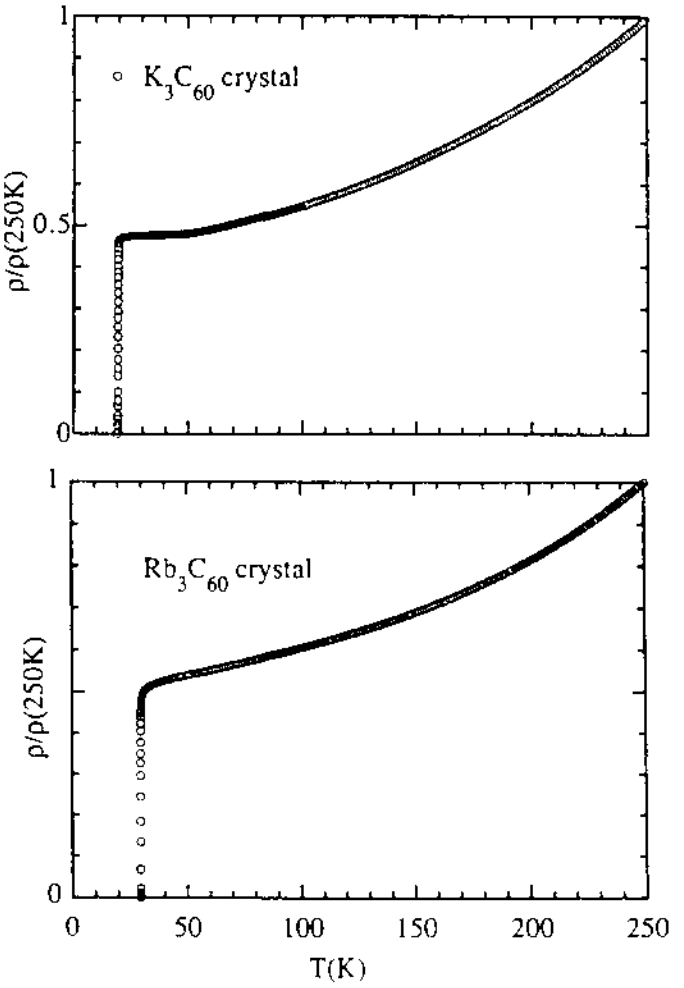

Figure 1: Normalized dc electrical resistivity of K_3C_{60} and Rb_3C_{60}.

form of $\rho(T)$ is in both cases clearly "metal-like", i.e. decreasing with decreasing temperature, there are some peculiarities. First, the residual resistivity ratio (RRR) is high, with $\rho(300)/\rho(0) \sim 2$ for both materials ($\rho(0)$ is the extrapolated zero temperature resistivity). Generally, the RRR is slightly higher for Rb_3C_{60} than for K_3C_{60}, suggesting more "disorder" in the Rb-doped system. Second, $\rho(T)$ shows unusual upward curvature over nearly the entire measured temperature range. Indeed, for both K_3C_{60} and Rb_3C_{60}, $\rho(T)$ is fit almost perfectly from just above T_c to well above room temperature by the functional form

$$\rho(T) = A + BT^2. \qquad (1)$$

Is the "T^2" fit meaningful? Very likely not. The large coefficient of thermal expansion in both materials implies that the density of states $N(E_F)$ is highly temperature dependent[3]. An accurate analysis of $\rho(T)$ thus necessitates a theoretical modeling of $N(E_F,T)$, or, more directly, a measurement of $\rho(T)$ under conditions of constant sample volume[4], not constant pressure. Both approaches have been used[3,5] and in each case $\rho(T)$ no longer obeys Eq. (1). $\rho(T)$ measured in Rb_3C_{60} under constant volume conditions is discussed in §2.4 .

Although the functional forms of $\rho(T)$ shown in Fig. 1 for K_3C_{60} and Rb_3C_{60} are quite reproducible from sample to sample, the absolute value of $\rho(300K)$ is somewhat sample dependent. The "best" single crystal specimens (presumably those with the most homogeneous doping) have $\rho_K(300K) \sim 1m\Omega$–cm and $\rho_{Rb}(300K) \sim 2m\Omega$–cm. Similar values are obtained for high quality films[6]. The uncertainties for the single crystal measurements are largely due to uncertainties in effective geometry.

Other methods have been applied to determine the absolute value of ρ. Extrapolated infrared reflectance measurements by Rotter et al[7] suggest for K_3C_{60} a low temperature resistivity $\rho(0) = 0.4$ mΩ-cm, and microwave surface impedance measurements again on K_3C_{60} by Klein et al[8] find $\rho(0) = 0.5$ mΩ-cm. It is also possible to determine $\rho(0)$ indirectly from an analysis of the fluctuation conductivity near T_c (see §2.2); this yields[2] $\rho_K(0) = 0.12$ mΩ-cm and $\rho_{Rb}(0) = 0.22$ mΩ-cm .

Perhaps the best approach in determining $\rho(0)$ is to apply the simple relation $\rho(0) = 4\pi/\omega_p^2\tau(0)$. An analysis of upper critical field data yields[9,10] values of the T=0 scattering time $\tau_K(0) = 1.7\pm0.5 \times 10^{-14}$s and $\tau_{Rb}(0) = 0.7\pm0.3 \times 10^{-14}$s. Combining this with theoretical values[11,12] of the plasma frequency, 1.2eV and 1.11eV respectively for K_3C_{60} and Rb_3C_{60}, we find $\rho_K(0) = 0.18\pm0.06$ mΩ-cm and $\rho_{Rb}(0) = 0.57\pm0.21$ mΩ-cm.

These values lie intermediate to those determined from direct single crystal and film dc resistivity measurements and those extracted from a fluctuation conductivity analysis; they imply "ideal sample" values for the room temperature resistivity $\rho_K(300K) \equiv 0.4$ mΩ-cm and $\rho_{Rb}(300K) \equiv 1.1$ mΩ-cm.

2.2 Low Temperature dc Resistivity: Paraconductivity Near T_c

In the normal state just above the thermodynamic superconducting phase transition temperature T_c, order parameter fluctuations can affect the normal state resistivity $\rho(T)$. In a conventional isotropic superconductor, such fluctuations are normally not observed since the temperature interval over which they exist is too small. The large intrinsic disorder in K_3C_{60} and Rb_3C_{60} extends the fluctuation temperature range such that it is experimentally accessible. In fact, A_3C_{60} superconductors have provided the first direct experimental test[2] of 3-D superconductivity fluctuation theory[13], dating to 1968!

Fig. 2 shows the dc resistivity of Rb_3C_{60} in the immediate temperature range above $T_c = 30.2K$[2]. The solid line is an extrapolation of the normal state $\rho(T)$; over this small temperature range a linear fit is adequate. The deviation of the experimental data from the extrapolated curve reflects the excess fluctuation conductivity σ' (i.e. paraconductivity), which from Aslamazov-Larkin theory[13] may be expressed as[14]

$$\sigma' = \sigma_{exc}\, t^{-(4-D)/2} \qquad (2)$$

where $\sigma_{exc} = 2\pi e^2/32h\xi(0)$, $t = (T-T_c)/T_c$, D is the dimensionality of the system, and $\xi(0)$ is the superconducting coherence length. The inset to Fig. 2 shows on a log-log plot the experimentally determined fluctuation conductivity σ' versus the reduced temperature t. A good fit is obtained for D=3, which indicates Rb_3C_{60} is an intrinsic three dimensional superconductor. Similar results are obtained for K_3C_{60}, where again D=3 provides the best fits. However, in K_3C_{60} there is evidence for an additional Maki-Thompson term[15] in the fluctuation conductivity with a pair-breaking parameter $\delta \approx 0.58$. In Rb_3C_{60}, the Maki-Thompson term can be neglected implying a larger δ, which in turn suggests a larger electron-phonon coupling in Rb_3C_{60}.

The fluctuation conductivity can be used to evaluate the intrinsic normal state residual resistivity, in a manner that eliminates sample

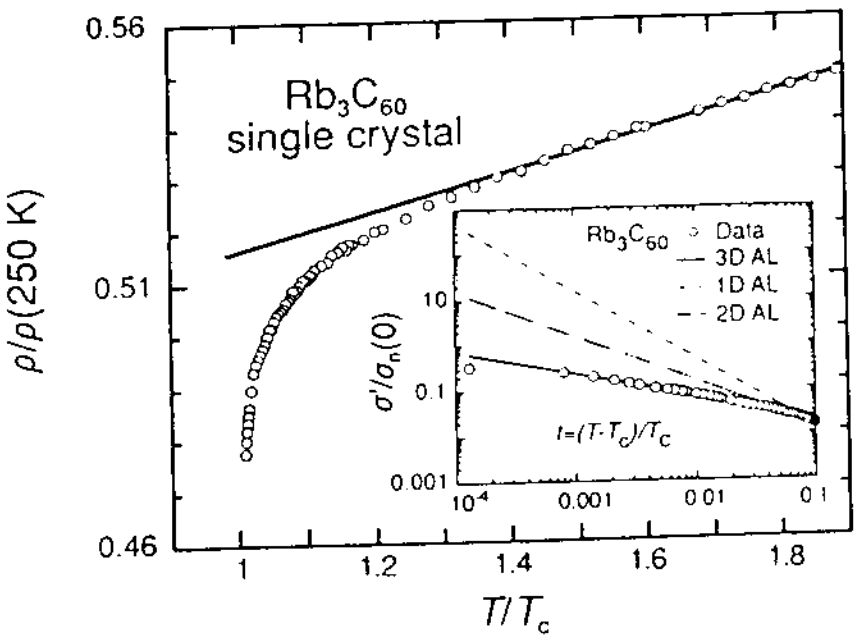

Figure 2: Dc resistivity of Rb_3C_{60} in the normal state near the superconducting phase transition. The solid line is an extrapolation of the normal state (fluctuation-free) resistivity. The inset shows the excess fluctuation conductivity versus reduced temperature. Aslamazov-Larkin fluctuation theory with a dimension D=3 provides an excellent fit to the data. The predicted curves for D=2 and D=1 are also shown.

geometry errors. With σ_n the measured normal state conductivity, geometry errors cancel in the ratio σ'/σ_n. Using $(\sigma_{exc}/\sigma_n)_K \approx 2\times10^{-3}$, $(\sigma_{exc}/\sigma_n)_{Rb} \approx 7.3\times10^{-3}$, $\xi(0)_K = 45$Å[9], and $\xi(0)_{Rb} = 24$Å[10], we obtain $\rho(0)_K \approx 0.12$ mΩ-cm and $\rho(0)_{Rb} \approx 0.22$ mΩ-cm. These values of $\rho(0)$ are comparable to but slightly smaller than those obtained from other measurement/analysis methods (see §2.1).

2.3 *High Temperature dc Resistivity: Saturation*

For a metal at high temperature, one might expect the resistivity to saturate as the scattering length (i.e. electronic mean free path) approaches the intrinsic interatomic distance. The high temperature resistivity of K_3C_{60} and Rb_3C_{60} has been examined[6,16] with this in mind.

Is the characteristic scattering length scale in A_3C_{60} the crystal lattice constant (~14Å) or the on-ball carbon-carbon distance (~1Å)?

Fig. 3 shows $\rho(T)$ measured[16] up to 800K in single crystal K_3C_{60} and up to 700K in single crystal Rb_3C_{60}. A pulsed heating technique has been used to prevent de-intercalation of the alkali metals at high temperature. $\rho(t)$ in K_3C_{60} accurately follows a T^2 temperature dependence all the way to 800K, while the data for Rb_3C_{60} show distinct curvature changes at high temperatures. Do these data sets indicate resistivity saturation? Naively one might expect resistivity saturation to manifest itself as a high temperature plateauing of $\rho(T)$; such behavior is clearly not observed for either material. However, the special properties of the alkali-fullerides necessitate a more careful theoretical treatment to confirm or exclude the observation of resistivity saturation.

As the electronic mean free path approaches the characteristic lattice spacing, Bloch-Boltzmann transport theory fails. One accounts for this effect by imposing a phenomenological minimum electron scattering time τ_{sat}, which corresponds to a length scale $\ell_{sat} = \tau_{sat} v_F$, on the order of the interatomic spacing. This minimal time acts as an offset to the Poisson distribution of electron scattering events, yielding a parallel resistor form[17,18] for the measured resistivity

$$\rho^{-1} = \rho_{BB}^{-1} + \rho_{sat}^{-1} \qquad (3)$$

where ρ_{BB} is the Bloch-Boltzmann resistivity; it is a sum of the residual resistivity ρ_o and the temperature-dependent electron-phonon resistivity ρ_{ep}. ρ_{ep}, given by the Ziman resistivity formula[18], incorporates the phonon spectrum and electron-phonon coupling. Furthermore, ρ_{ep} is proportional to $[N(E_F)]^2$. The strong temperature dependence of the density of states in A_3C_{60} conductors must be taken into account in an analysis of the resistivity.

Hou et al[16] have performed a careful analysis of the high temperature resistivity of K_3C_{60} and Rb_3C_{60}, by applying Eq. (3). A temperature-dependent density of states is used and different model forms of the phonon spectral function are tested. Fig. 4 compares the results of the theoretical analysis to the experimental data. For Rb_3C_{60}, a good fit is obtained using a model coupling spectrum[19] with average phonon frequency $\langle\omega\rangle \approx 2000$K (a fit using a model coupling spectrum[20] with $\langle\omega\rangle \approx 500$K yields an inferior fit). The analysis indicates resistivity saturation and yields $\rho_{sat} = 6.3 \pm 2.4$ mΩ-cm. With $v_F = 1.6 \times 10^7$ cm/sec, we obtain $\ell_{sat} = 1.0 \pm 0.5$ Å. In Rb_3C_{60}, the saturation length is on the order

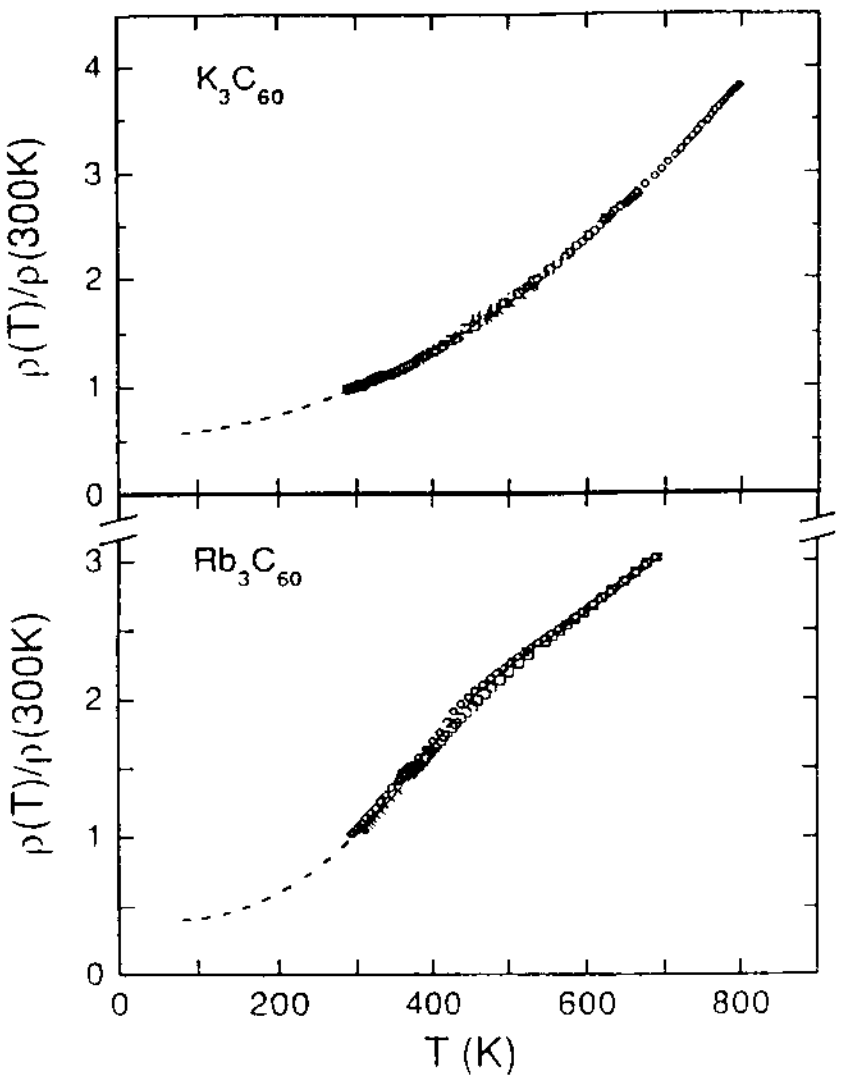

Figure 3: Resistivity of K_3C_{60} and Rb_3C_{60} over an extended temperature range. Different symbols correspond to different pulsed heating runs. Data below 300K (dashed lines) were obtained using conventional slow cooling methods.

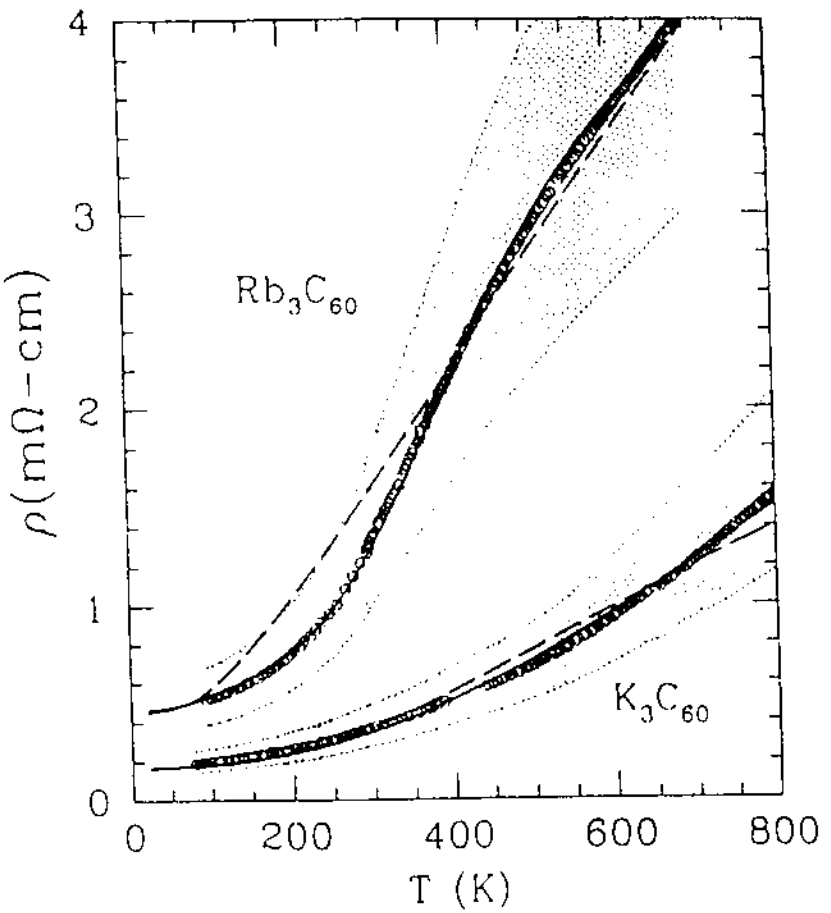

Figure 4: Resistivity versus temperature for Rb_3C_{60} (upper curves) and K_3C_{60} (lower curves) Open circles represent experimental data normalized to $\rho_K(0) = 0.18$ mΩ-cm and $\rho_{Rb}(0) = 0.57$ mΩ-cm. Shaded regions indicate uncertainties in absolute resistivity normalization. The solid and dashed lines are theoretical fits[16] from which resistivity saturation parameters are extracted. For Rb_3C_{60} the dashed line fit uses the electron-phonon coupling spectrum from Jishi et al [20]($\langle\omega\rangle \approx 500$K), while the solid line fit uses the spectrum of Varma et al[19] ($\langle\omega\rangle \approx 2000$K). Both models include a temperature dependent density of states. The fits to the K_3C_{60} data use the coupling spectrum from Schluter et al[21] ($\langle\omega\rangle \approx 1200$K). The solid line includes a temperature-dependent density of states whereas the dashed fit does not.

of the carbon-carbon bond length. Fig. 4 also shows the theoretical fit to the K_3C_{60} data. The data do not show obvious signs of resistivity saturation, but the analysis, using a model coupling spectrum[21] with $\langle\omega\rangle \approx 1200$K, yields a lower bound on the magnitude of the saturation resistivity: $\rho_{sat} > 3m\Omega$-cm and $\ell_{sat} < 1.5$Å. The characteristic saturation length in K_3C_{60} is expected to be again on the order of the carbon-carbon bond length.

The high-temperature resistivity measurements and analysis suggest that the single particle states relevant to transport at high temperatures in A_3C_{60} have a length scale much smaller than the fcc lattice constant or the C_{60} ball nearest neighbor center-to-center distance. Although the extended-state description of electronic dynamics may be applicable to A_3C_{60} at low temperatures, the small saturation scattering length implies that the character of the appropriate electronic states at high temperatures is quite different.

2.4 *Pressure Studies: Constant-volume $\rho(T)$*

As mentioned above, the large thermal expansion of A_3C_{60} complicates direct comparison of transport measurements with theoretical model predictions. Model predictions usually assume a constant sample volume, while most experiments are carried out under constant pressure conditions. Crespi et al[3] and Hou et al[16] have compared experimental constant-pressure $\rho(T)$ data of K_3C_{60} and Rb_3C_{60} to various electron-phonon scattering models incorporating a temperature-dependent density of states $N(E_F)$. One such comparison has been shown in Fig. 4.

Here we adopt a different strategy: a direct experimental determination of the constant-volume $\rho(T)$, which we designate $\rho_v(T)$. This is possible by applying external, hydrostatic pressure to the sample to prevent thermal expansion. In an ideal experiment, the pressure would be adjusted at each temperature so as to compensate for thermal expansion and bring the sample volume to a chosen reference volume v_o, say the ambient pressure volume at 4.2K. In practice the volume of the sample is not measured directly but is inferred from the applied pressure and the independently determined (temperature dependent) bulk modulus. In addition, in a typical experiment $\rho(T)$ is determined as a function of temperature only for a series of semi-temperature-independent "clamp" pressures; the data are then interpolated to determine $\rho_v(T)$.

Fig. 5 shows the result of $\rho_v(T)$ determined for a Rb_3C_{60} crystal[5]. The maximum pressure applied, at 350K, is about 8kbar. From 100K to 350K,

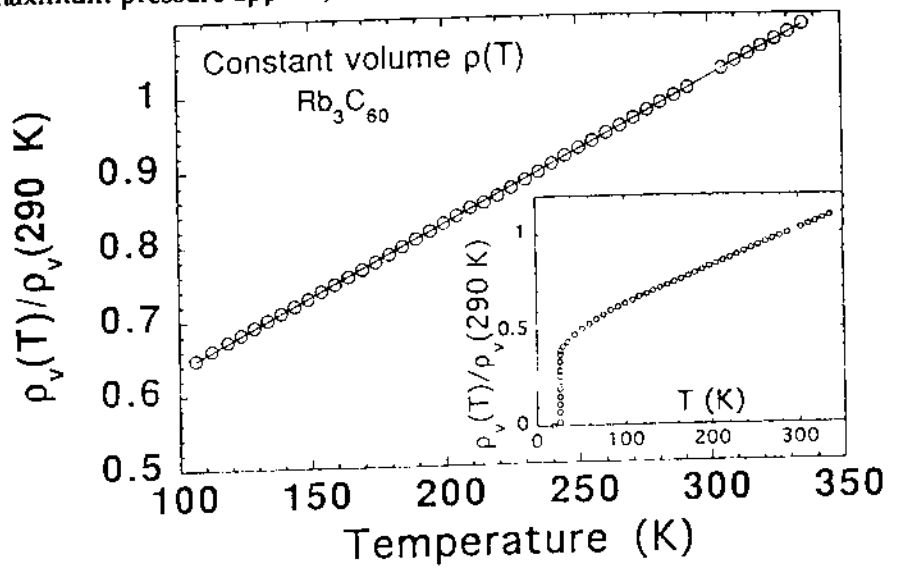

Figure 5: Constant sample volume resistivity versus temperature for Rb_3C_{60}. A linear temperature dependence is apparent. The inset shows the constant volume resistivity over an extended temperature range, but data at lower temperatures become less reliable due to increasing uncertainties in the data corrections applied.

the $\rho_v(T)$ data differ significantly from the "constant pressure" T^2 result of Eq. (2). Instead, for constant sample volume a *linear* temperature dependence is observed, i.e.

$$\rho_v(T) = a + bT. \qquad (4)$$

This is the "intrinsic" resistivity of Rb_3C_{60}. The inset to Fig. 5 shows $\rho_v(T)$ over an extended temperature range. The data near T_c are not reliable due to uncertainties in the data correction at low temperatures.

In the higher temperature regime, the slope of the $\rho_v(T)$ curve, $d\rho/dT$, is directly related to the transport electron-phonon coupling constant λ_{tr}. Combining $\rho(T) = 4\pi/\omega_p^2\tau$ with the first term in the scattering time expansion (valid for $T>\theta_D$), $\tau^{-1} = \lambda_{tr}k_BT/h$, we obtain

$$\lambda_{tr} = (h\omega_p^2/16\pi^3k_B)\, d\rho/dT = 0.246\,(h\omega_p/2\pi)^2\, d\rho/dT, \qquad (5)$$

the later equality holding with units $[d\rho/dT] = \mu\Omega$-cm/K and $[\hbar\omega_p/2\pi] =$ eV. The relative slope of $\rho_v(T)$ in Fig. 5 is $(1/\rho_o)d\rho/dT \approx (1.9 - 2.2) \times 10^{-3}$ K^{-1}. To obtain $d\rho/dT$, ρ_o, i.e. $\rho_{Rb}(295K)$, must be known. From §2.1 we have $\rho_o \approx 1.1 m\Omega$-cm, which, with a plasma frequency of 1.2eV, leads to $\lambda_{tr} \approx 0.30$-$0.35$. The directly measured crystal $\rho_{Rb}(295K) = 2.5$ mΩ-cm leads to $\lambda_{tr} \approx 0.65$-$0.80$.

It is interesting to note that, identifying λ_{tr} with the superconductivity electron-phonon coupling constant λ, the evaluated range of λ_{tr}'s is entirely consistent with a 30K superconducting transition temperature, assuming a conventional phonon-mediated electron-electron pairing mechanism with characteristic phonon frequencies of order 2000K. It is not necessary to invoke "exotic" scattering or superconductivity mechanisms to account for the measured $\rho(T)$ or T_c in Rb_3C_{60}.

2.5 Hall Effect

For A_3C_{60}, we might expect that the intercalated alkali atoms donate one electron each to the host C_{60} structure, leading to 3 free electrons per C_{60}. In the most elementary (free electron) model, the Hall coefficient is given by $R_H = -1/nec$, with n the carrier concentration. With 3 electrons/C_{60}, $R_H = -1.4 \times 10^{-9}$ m^3/C.

Fig. 6 shows R_H (T) determined[22] for single crystal K_3C_{60} and Rb_3C_{60}.

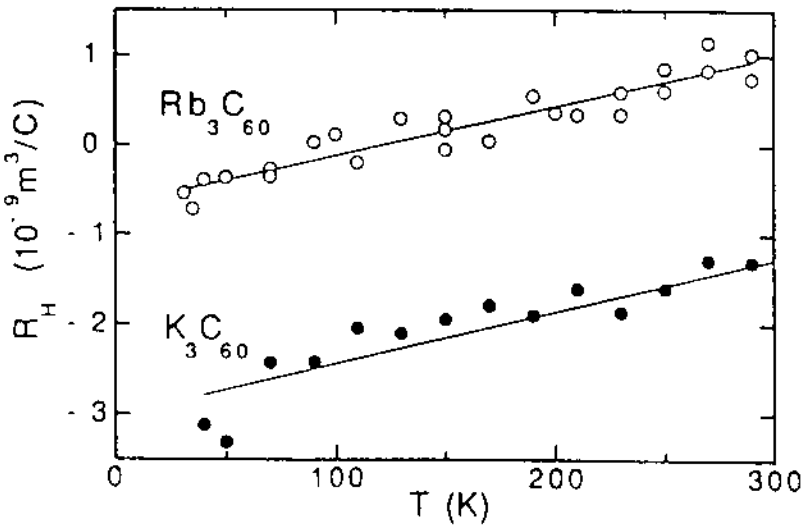

Figure 6: Hall coefficient for K_3C_{60} and Rb_3C_{60}.

For K_3C_{60}, R_H at room temperature is -1.4×10^{-9} m^3/C, which coincides with the free electron result with 3 electrons/C_{60}. This coincidence is most likely fortuitous; the free electron model is of limited utility in a system with a complex Fermi surface. Over the measured temperature range, R_H for K_3C_{60} is negative and increases linearly with increasing temperature with a slope 0.0055×10^{-9} m^3/CK. For Rb_3C_{60}, R_H again increases linearly with temperature with the same slope; the data are displaced upward from those of K_3C_{60} and there is a zero crossing at T~120K.

The observation of a strong influence of thermal expansion on the dc electrical resistivity of A_3C_{60} suggests that lattice thermal expansion should be taken into account in a discussion of $R_H(T)$. The lattice thermal expansion of A_3C_{60} in the temperature range of interest can be adequately expressed as $a(T) = a_o + bT$, where b is 3.52×10^{-4} Å/K for K_3C_{60}[23] and 4.4×10^{-4} Å/K for Rb_3C_{60}[24].

Fig. 7 shows R_H versus lattice constant a. This striking relationship

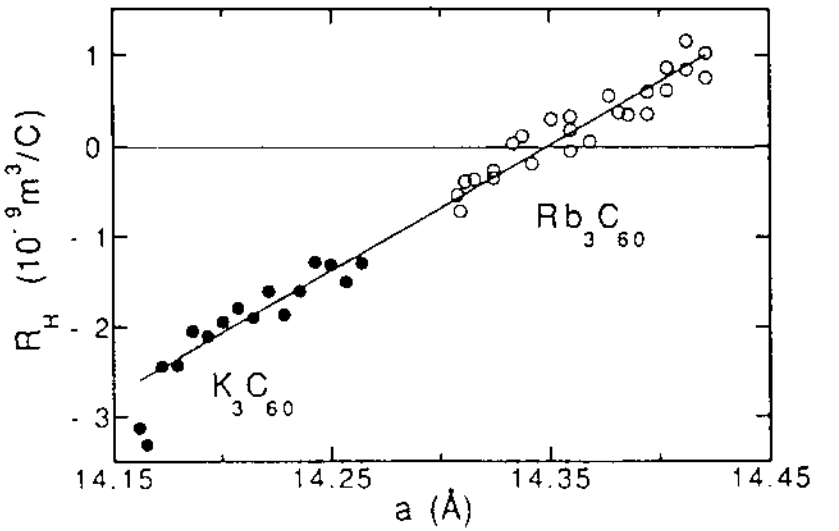

Figure 7: Hall coefficient for K_3C_{60} and Rb_3C_{60} plotted as a function of lattice constant. A universal function for R_H is observed, suggesting that R_H, at constant sample volume, is temperature and material independent.

shows that the difference in R_H between K_3C_{60} and Rb_3C_{60} at a given temperature can be ascribed purely to the difference in the lattice constant between the two materials, and that the temperature dependence of R_H in the two materials can also be ascribed purely to changes in the lattice constant. In other words, R_H at constant sample volume is temperature

independent for both materials. For both K_3C_{60} and Rb_3C_{60}, the experimentally determined Hall coefficient can be expressed as

$$R_H = [-2.8 + 13.9(a - 14.15)] \times 10^{-9}\ m^3/C, \quad (6)$$

where a is measured in angstroms. Eq. (6) is expected to hold for *all* A_3C_{60} conductors, including mixed alkali alloys, although this prediction has not been tested.

Prior calculations by Erwin and Pickett[25] of the Hall coefficient in A_3C_{60} using the Jones-Zener solution of the Boltzmann equation in an orientationally ordered system at T=0 with isotropic scattering time yield $R_H = 7 \times 10^{-9}\ m^3/C$ for both K_3C_{60} and Rb_3C_{60}. This result, which is weakly pressure dependent, arises from a complex weighted average of curvature over the Fermi surface. However, this prediction is inconsistent with the data of Figs. 6 and 7. The experiments show R_H to be smaller in absolute magnitude and negative over a wide temperature range. Furthermore, Eq. (6) suggests a pressure dependence to R_H much stronger than that calculated. Since R_H is sensitive to details of the Fermi surface curvature, it is likely that the discrepancy between theory and experiment is due to disorder-induced modification of the Fermi surface (not taken into account in the orientationally ordered calculation).

Lu et al[22] have modeled the effects of lattice-constant-dependent disorder broadening at the Fermi level. The variation in R_H with lattice constant is accounted for by assuming that the relative k-space extent of the disorder broadening of the Fermi surface increases with increasing lattice constant. If the effects of the disorder have a characteristic energy scale which is to lowest order independent of the lattice constant, then the k-space extent of the disorder broadening will be an increasing function of the density of states at the Fermi level and hence an increasing function of the lattice constant. This goes hand in hand with the larger dc residual resistivity of Rb_3C_{60} compared to K_3C_{60} (§2.1). The behavior is similar to that suggested for disordered nearly free electron metals, wherein R_H is inversely dependent on the density of states[26].

The model of Lu et al predicts that the Hall coefficient R_H in A_3C_{60} will increase from negative values at low disorder broadening to positive values at larger disorder broadening. This is consistent with the experimental results, which show negative R_H for the K_3C_{60} sample at low T (small density of states) going over to positive R_H for the Rb_3C_{60} sample at high T (large density of states). A simplified calculation[22] applying the disorder-broadening model predicts the correct ratio of the extrapolated T=0 Hall coefficients of K_3C_{60} and Rb_3C_{60}.

2.6 Thermoelectric Power

For a conventional metal, the thermoelectric power (TEP) is expected to be small in magnitude (order μV/K), have a sign reflecting the sign of the charge carriers, and be linear in temperature.

Fig. 8 shows the TEP for K_3C_{60} and Rb_3C_{60} as measured by Inabe et al[27]. These crystals have been grown from a CS_2 solution and they display an anomalously high resistivity, suggesting incomplete doping or CS_2 impurities. However, the TEP results are consistent with those obtained[28] on vapor-transport grown crystals. The data of Fig. 8 indicate a linear TEP for both materials, with room temperature values -10 μV/K for K_3C_{60} and -15μV/K for Rb_3C_{60}. The hump structure near 50K in both materials may be due to phonon drag. The TEP results are consistent with metallic behavior.

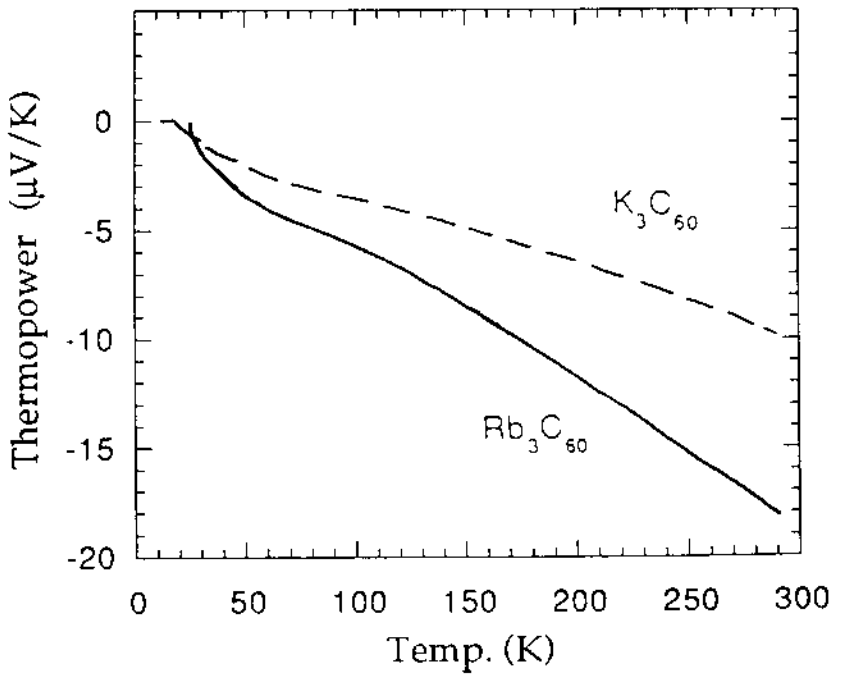

Figure 8: Thermoelectric power versus temperature for K_3C_{60} and Rb_3C_{60}. After Inabe et al[27].

Inabe et al have used the TEP results to estimate the density of states ratio between Rb_3C_{60} and K_3C_{60}; they obtain[27] $N_{Rb}(E_F)/N_K(E_F)$ = 1.5-1.8. Band structure calculations[29] indicate a somewhat smaller density of states ratio of ~1.2.

3 Transport in A_1C_{60}

The recently discovered polymerized A_1C_{60} materials have been characterized by a variety of techniques, including structural[30], Raman[31], IR[32], and spin resonance[33]. The structure is intriguing in that it consists of C_{60} molecules covalently bonded into linear chains. Although such a geometry is a template for quasi-one-dimensional conduction, the actual charge transport in these materials may be quite complicated. For example, the C_{60}-C_{60} bond is expected to be a serious impediment to charge conduction, and transport along the chain axis may actually follow a "zig-zag" path where charges hop from one polymerized chain to another.

Clearly transport measurements in single crystal specimens would be highly desirable. Unfortunately, even the best available samples of A_1C_{60} (A=K,Rb,Cs) are not true single crystals, in that the polymerization direction is not uniform throughout the macroscopic specimen. Hence all transport measurements to date on the A_1C_{60} materials represent an average over different crystal directions and cannot distinguish crystal anisotropies. Nevertheless, such measurements are illuminating and show a rich electronic structure.

3.1 Dc Resistivity of A_1C_{60}

Fig. 9 shows the dc electrical resistivity $\rho(T)$ of K_1C_{60} from room temperature to 4K. Between 300K and 50K a metal-like behavior is observed, with $\rho(T)$ decreasing smoothly with decreasing temperature. However, $\rho(T)$ does not follow any conventional form (the solid line in the figure is fit to the functional form $A + BT + CT^2$). It is possible that thermal expansion plays a role in the observed $\rho(T)$, although in this covalently-bonded polymer the effect is expected to be less severe than in A_3C_{60} compounds.

Below 50K, the resistivity of K_1C_{60} is anomalous and increases with decreasing temperature. This may be the signature of a structural and/or electronic phase transition. For example, the spin density wave (SDW)

transition in the low dimensional organic charge transfer salt $(TMTSF)_2PF_6$ manifests itself as a very similar upturn in $\rho(T)$[35]. The low temperature resistivity in K_1C_{60} does not, however, follow any activated form as might be expected with the opening of a gap at the Fermi energy. If the 50K transition in A_1C_{60} is associated with formation of a SDW (or, alternatively, a charge density wave), then the Fermi surface is most

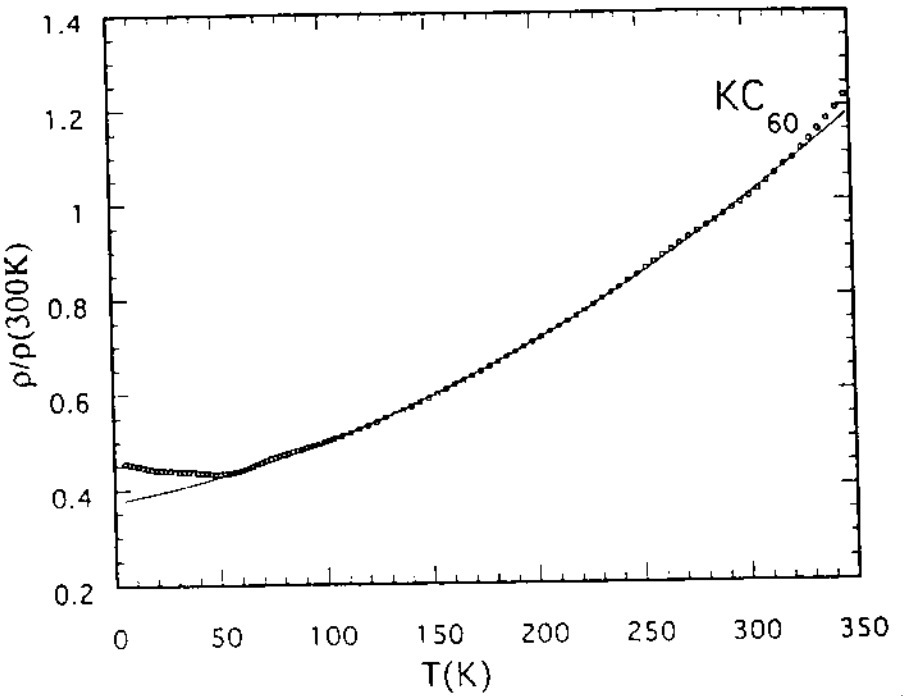

Figure 9: Dc electrical resistivity versus temperature in K_1C_{60}. An apparent phase transition occurs near 50K.

likely only partially gapped. In K_1C_{60}, no superconductivity is observed down to 1.9K under ambient pressure conditions. In addition, no magnetoresistance is observed (using fields up to 7T) at any temperature.

Fig. 10 shows the dc resistivity for Rb_1C_{60}[36] and Cs_1C_{60}[37]. For both materials, the transport properties indicate semiconducting, rather than metallic, behavior. Activated behavior with a temperature-independent activation energy is not observed. A careful examination of the $\rho(T)$ curve

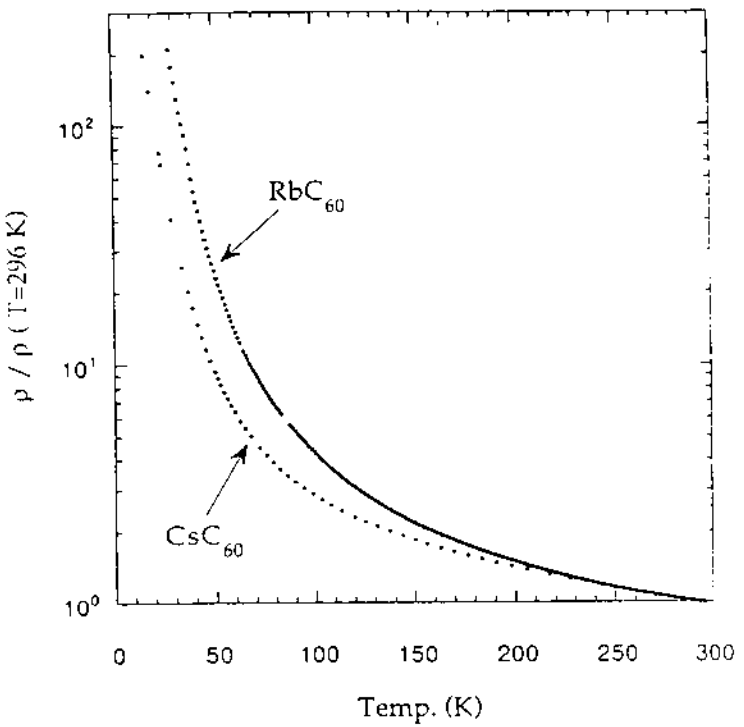

Figure 10: Dc electrical resistivity of Rb_1C_{60} and Cs_1C_{60} versus temperature.

for Rb_1C_{60} indicates a subtle anomaly near 50K. ESR[33] and IR[32] transmission measurements show evidence for a low temperature phase transition in Rb_1C_{60}. In the IR studies, the phase transition is identified at 34K, while the ESR anomaly occurs at around 50K. Assuming only one transition, the origin of the temperature discrepancy is not clear. It is likely that this transition is associated with a SDW or other spin reordering, and that the anomaly in the dc resistivity reflects the same transition.

3.2 Pressure Effects on the dc Resistivity

The dc resistivity of K_1C_{60} is extremely pressure dependent. At room temperature, an applied hydrostatic pressure of 15kbar reduces the resistivity by 70%[34]. A further increase in pressure has little effect. This suggests a saturation in the charge transfer matrix element (possibly inter-chain hopping). The electrical resistivity measured[34] under such "saturation" conditions is shown in Fig. 11. A fully conventional metallic $\rho(T)$ is observed, with no evidence for a low temperature phase transition. No superconductivity is observed to 4.2K (14.5kbar). It is likely that applied pressure makes K_1C_{60} more three-dimensional, hence suppressing the quasi 1-D low temperature magnetic phase transition.

Pressure studies have also been recently been performed[36,37] on Rb_1C_{60} and Cs_1C_{60}. The semiconducting $\rho(T)$ is transformed into a metal-like $\rho(T)$, with sharp "semiconductor-to-metal" transitions observed with decreasing temperature at fixed pressures. These transitions suggest a rich electronic/magnetic phase diagram for the A_1C_{60} polymers. Additional transport and structural measurements, if possible on single domain samples, would be highly desirable.

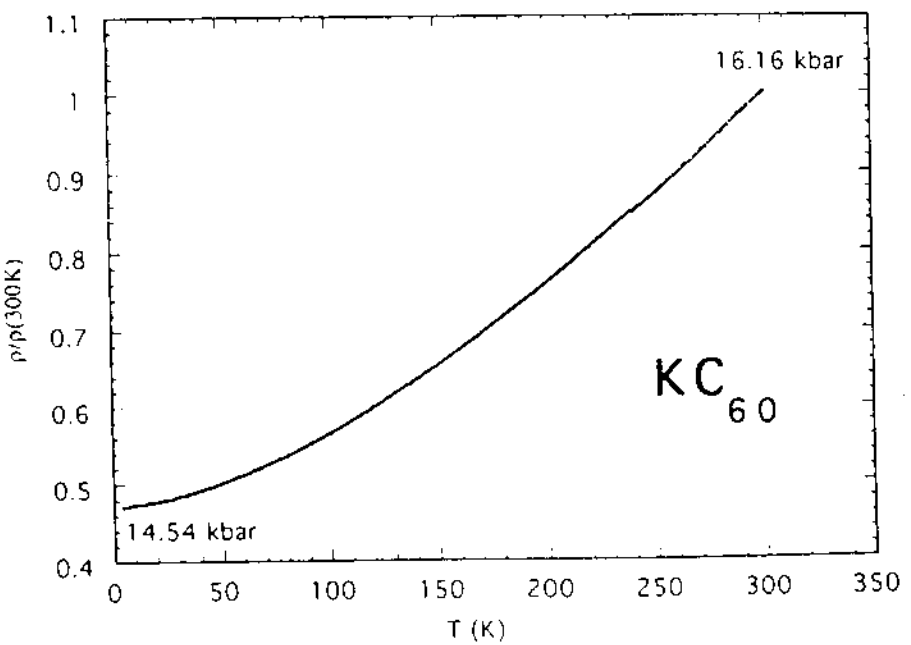

Figure 11: High-pressure dc electrical resistivity of K_1C_{60}. Metallic behavior is observed over the entire measured temperature range.

Acknowledgments

This work was performed in collaboration with G. Briceno, M.L. Cohen, V. H. Crespi, M.F. Fuhrer, J. Hone, J.G. Hou, K. Khazeni, L. Lu, W. Vareka, and X.-D. Xiang. Support is acknowledged from NSF Grant DMR-94-04755 and DOE grant DE-AC03-76F00098. AZ received support from the Miller Institute for Basic Research in Science.

References

1. X.-D. Xiang, J.G. Hou, G. Briceno, W.A. Vareka, R. Mostovoy, A. Zettl, V.H. Crespi, and M.L. Cohen, *Science* **256**, 1190 (1992)
2. X.-D. Xiang, J.G. Hou, V.H. Crespi, A. Zettl, and M.L. Cohen, *Nature* **361**, 54 (1993)
3. V.H. Crespi, J.G. Hou, X.-D. Xiang, M.L. Cohen, and A. Zettl, *Phys. Rev. B***46**, 12064 (1992)
4. B. Sundqvist and B. M. Andersson, *Solid State Commun.* **76**, 1019 (1990)
5. W.A. Vareka and A. Zettl, *Phys. Rev. Lett.* **72**, 4121 (1994)
6. A.F. Hebard, T.T. M. Palstra, R.C. Haddon, and R.M. Fleming, *Phys. Rev. B***48**, 9945 (1993)
7. L.D. Rotter, Z. Schlesinger, J.P. McCauley, Jr., N. Coustel, J.E. Fischer, and A.B. Smith III, *Nature* **355**, 532 (1992)
8. O. Klein, G. Gruner, S.-M. Huang, J.B. Wiley, and R.B. Kaner, *Phys. Rev. B***46**, 11247 (1992)
9. J. G. Hou, V.H. Crespi, X.-D. Xiang, W.A. Vareka, G. Briceno, A. Zettl, and M.L. Cohen, *Solid State Commun.* **86**, 643 (1993)
10. J.G. Hou, X.-D. Xiang, V.H. Crespi, M.L. Cohen, and A. Zettl. *Physica C* **228**, 175 (1994)
11. S.C. Erwin and W.E. Pickett, *Science* **254**, 842 (1991)
12. S.C. Erwin (personal communication to V.H. Crespi)
13. L.G. Aslamasov and A.I. Larkin, *Phys. Lett. A***26**, 238 (1968)
14. W. J. Skocpal and M. Tinkham, *Rep. Prog. Phys.* **38**, 1049 (1975)
15. K. Maki, *Prog. Theor. Phys.* **39**, 887 (1968); **40**, 193 (1968); R.S. Thompson, *Phys. Rev. B***1**, 327 (1970); *Physica* **55**, 296 (1971); K. Maki and R.S. Thompson, *Phys. Rev. B***39**, 2767 (1989)
16. J.G. Hou, L. Lu, v.H. Crespi, X.-D. Xiang, A. Zettl, and M.L. Cohen, *Solid State Commun.* **93**, 973 (1995)

17. P.B. Allen in *Superconductivity in d-and f-Band Metals*, ed H. Suhl and M.B. Maple (Academic Press, New York, 1980) p. 291; M. Gurvich, *Phys. Rev. B***24**, 7407 (1981)
18. G. Grimvall in *The Electron-phonon Interaction in Metals* (NorthHolland, 1991) pp. 210-223
19. C.M. Varma, J. Zaanen, and K. Raghavachari, *Science* **245**, 989 (1991)
20. R.A. Jishi and M.S. Dresselhaus, *Phys. Rev. B***45**, 2597 (1992)
21. M. Schluter, M. Lannoo, M. Needles, and G.A. Baraff, *Phys. Rev. Lett.* **68**, 526 (1992)
22. L. Lu, V.H. Crespi, M.S. Fuhrer, A. Zettl, and M.L. Cohen, *Phys. Rev. Lett.* **74**, 1637 (1995)
23. Q. Zhu and J.E. Fisher (private communication)
24. O. Zhou et al in *Novel Froms of Carbon*, eds. C.L. Renschler, J.J. Pouch, and d.M. Cox (Materials Research Society, San Francisco, 1992) vol. 270, p. 191
25. S.C. Erwin and W.E. Pickett, *Phys. Rev. B***46**, 14257 (1992)
26. J.M. Ziman, *Adv. Phys.* **13**, 578 (1967)
27. T. Inabe, H. Ogata, Y. Maruyama, Y. Achiba, S. Suzuki, K. Kikuchi, and I. Ikemoto, *Phys. Rev. Lett.* **69**, 3797 (1992)
28. L. Lu, M.F. Fuhrer, and A. Zettl (to be published)
29. S. Saito and A. Oshiyama, *Phys. Rev. B***44**, 11536 (1991)
30. P.W. Stephens et al, *Nature* **370**, 636 (1994)
31. H. Kuzmany, T. Pichler, R. Winkler, and M. Haluska, in *Physics and Chemistry of Fullerenes and Derivatives*, eds H. Kuzmany, J. Fink, M. Mehring, and S. Roth (World Scientific, Singapore, 1995) p. 340
32. J. Winter and H. Kuzmany, *Solid State Commun.* **84**, 935 (1992); M.C. Martin, D. Koller, A. Rosenberg, C. Kendizora, and L. Mihaly, *Phys, Rev. B***51**, 3210 (1995)
33. O. Chauver, G. Oszlanyi, L. Forro, P.W. Stephens, M. Tegze, G. Faigel, and A. Janossy, *Phys. Rev. Lett.* **72**, 2721 (1994)
34. J. Hone, M.S. Fuhrer, K. Khazeni, and A. Zettl, *Phys. Rev. B***52**, R8700 (1995)
35. P.M. Chaikin, G. Gruner, E.M. Engler, and R. L. Greene, *Phys. Rev. Lett* **45**, 1874 (1980), and references therein
36. K. Khazeni, J. Hone, and A. Zettl, (to be published)
37. J. Hone, K. Khazeni, and A. Zettl, (to be published)